

# Anomalous effective charges and far IR optical absorption of $\text{Al}_2\text{Ru}$ from first principles

Serdar Ögüt\* and Karin M. Rabe

*Department of Physics, Yale University*

*P. O. Box 208120, New Haven, Connecticut, 06520-8120*

(October 25, 2018)

## Abstract

For the orthorhombic intermetallic semiconductor  $\text{Al}_2\text{Ru}$ , the bandstructure, valence charge density, zone center optical phonon frequencies, and Born effective charge and electronic dielectric tensors are calculated using variational density functional perturbation theory with *ab initio* pseudopotentials and a plane wave basis set. Good agreement is obtained with recent measurements on polycrystalline samples which showed anomalously strong far IR absorption by optical phonons, while analysis of the valence charge density shows that the static ionic charges of Al and Ru are negligible. Hybridization is proposed as the single origin both of the semiconducting gap and the anomalous Born effective charges. Analogous behavior is expected in related compounds such as NiSnZr, PbTe, skutterudites, and Al-transition-metal quasicrystals.

78.30.Hv, 71.20.Lp, 63.20.Dj

Typeset using REVTeX

Al<sub>2</sub>Ru is an intermetallic semiconductor<sup>1</sup> quite close in composition to the Al-transition-metal quasicrystals. Because of its relatively simple crystal structure, it has been suggested<sup>2,3</sup> that investigation of Al<sub>2</sub>Ru can contribute to the understanding of the pseudogap in the electronic density of states observed in quasicrystals. From first-principles calculations of the bandstructure and charge density performed using linear-muffin-tin-orbitals (LMTO) in the atomic sphere approximation,<sup>2</sup> it has been shown that the fundamental gap results from the hybridization of  $sp(\text{Al})$  and  $d(\text{Ru})$  states. More recently, hybridization has been identified as the origin of the pseudogap in other aluminum-rich transition-metal compounds.<sup>4,5</sup>

This high degree of hybridization in states near the fundamental gap might be expected to have implications for other properties as well. In perovskite-structure oxides, it has been shown that hybridization between oxygen  $p$  orbitals and transition-metal  $d$  orbitals results in values for Born effective charges much larger than the nominal ionic values.<sup>6,7,8</sup> In Al<sub>2</sub>Ru, experimental measurement of the optical conductivity shows a strikingly large oscillator strength for phonon absorption.<sup>3,9</sup> The estimated values of Born effective charges, comparable to those of typical ionic insulators, are very much larger than the static ionic charges, which previous calculation<sup>2</sup> has shown to be negligible. In this paper, we report the first-principles calculation of the zone-center phonon frequencies, the Born effective charges, and the dielectric tensor of Al<sub>2</sub>Ru. We obtain good agreement for the far-infrared optical conductivity with the experimental measurements. Confirming that the static charge transfer between Al and Ru is negligible, we conclude that hybridization may be responsible for the large effective charges, providing a single mechanism linking the formation of the semiconducting gap and the observed strong phonon optical absorption in the far IR.

The first principles calculations were performed using the *ab initio* pseudopotential method with a plane wave basis set and the conjugate gradients algorithm.<sup>10</sup> For Al, we used Hamann-Schlüter-Chiang pseudopotentials<sup>11</sup> with reference configuration  $3s^13p^13d^1$  and cutoff radii of 1.1, 1.2, and 1.3 a.u. For Ru, we constructed scalar relativistic optimized pseudopotentials<sup>12</sup> with reference configuration  $5s^{1.75}5p^{0.25}4d^6$ , and cutoff radii of 2.2, 2.4, and 2.05 a.u. The pseudowavefunctions for  $s$ ,  $p$ , and  $d$  orbitals were expanded using 3,

4, and 6 Bessel functions with  $q_c$ 's of 4, 4, and  $6.05\sqrt{Ry}$ , respectively. The pseudopotentials were put into separable form with two projectors<sup>13</sup> for each angular momentum with the  $l = 0$  component taken as local for both Al and Ru. The energy cutoff was taken as 500 eV, resulting in a kinetic energy convergence of 2 mRy. The local density approximation (LDA) was used with the exchange-correlation functional of Ceperley and Alder as parametrized by Vosko, Wilk and Nusair.<sup>14</sup> The conjugate gradients minimization for the self-consistent charge density and bandstructure was performed using the program CASTEP 2.1. The force constants, Born effective charge tensors  $Z_{\kappa,\alpha\beta}^*$ , and the dielectric tensor  $\epsilon_\infty$  were computed using the density functional perturbation theory method<sup>15</sup> in the variational formulation.<sup>16</sup> All calculations were performed for the experimentally observed face-centered orthorhombic structure with six atoms per unit cell (space group  $Fddd$ ), lattice constants  $a = 8.015 \text{ \AA}$ ,  $b = 4.715 \text{ \AA}$ , and  $c = 8.780 \text{ \AA}$ , and free structural parameter  $x = \frac{1}{3}$ .<sup>17</sup> The special  $\mathbf{k}$ -point set was a  $4 \times 6 \times 4$  Monkhorst-Pack grid<sup>18</sup> in the Brillouin zone (BZ) of a simple orthorhombic lattice with lattice constants  $\frac{a}{2}$ ,  $\frac{b}{2}$ , and  $\frac{c}{2}$ , folded in to obtain 48  $\mathbf{k}$  points in the full BZ of the primitive face-centered orthorhombic lattice [Fig. 1(a)]. The acoustic sum rule for phonons and charge neutrality for  $Z_{\kappa,\alpha\beta}^*$  were imposed by adding small corrections ( $\leq 1\%$ ) to the largest matrix elements in each case.

The first-principles bandstructure of  $\text{Al}_2\text{Ru}$  is shown in Fig. 1(b), with the main features in good agreement with previously calculated bandstructures.<sup>2,19</sup> At the bottom of the valence band are free-electron-like bands derived mainly from Al  $s$  states. In the upper half of the valence band, flat bands derived from Ru  $d$  states are seen to be strongly hybridized with the more dispersive Al  $s$  and  $p$  bands. These calculations show that  $\text{Al}_2\text{Ru}$  is a semiconductor, with a 0.35 eV indirect band gap from  $\Gamma$  to the conduction band minimum along  $\Gamma - B$ . The total valence charge density in the  $z = 0$  plane, shown in Fig. 2(a), is quite similar to the valence charge density of superimposed free neutral atoms. The difference, shown in Fig. 2(b), can be characterized as a small shift of charge from the core regions into the interstitial region between the Al and Ru atoms. From this, it seems clear that there is no significant charge transfer between Al and Ru, and therefore, negligible ionic character

for the bonding in this compound.

From our first-principles computations of the dielectric tensor, we obtain

$$\epsilon_{\infty} = \begin{pmatrix} 18.9 & 0 & 0 \\ 0 & 22.9 & 0 \\ 0 & 0 & 20.7 \end{pmatrix} \quad (0.1)$$

These large values are characteristic of narrow-gap semiconductors, such as PbTe, with  $\epsilon_{\infty} = 32.8$ .<sup>20</sup> From computations of the Born effective charge tensors  $Z_{\kappa,\alpha\beta}^* = \partial P_{\alpha} / \partial u_{\kappa,\beta}$ , we find for Ru, with site symmetry 222,

$$Z_{Ru}^* = \begin{pmatrix} -6.28 & 0 & 0 \\ 0 & -6.96 & 0 \\ 0 & 0 & -5.40 \end{pmatrix} \quad (0.2)$$

For Al, in the lower symmetry site 2..., we find

$$Z_{Al}^* = \begin{pmatrix} 3.14 & 0 & 0 \\ 0 & 3.48 & \pm 0.70 \\ 0 & \pm 0.47 & 2.70 \end{pmatrix} \quad (0.3)$$

where the plus/minus signs refer to the two different orientations of the nearest neighbor shell for symmetry-related Al atoms. In contrast to the negligible static ionic charges, these dynamical effective charges correspond in magnitude to a complete transfer of the fourteen valence electrons per unit cell to Ru, leaving the Al ions with an effective charge of +3. The phonon absorption is determined by these dynamical charges, and not by the static ionic charges, accounting for the large oscillator strength observed in Al<sub>2</sub>Ru.

To compare these results quantitatively with the measured optical conductivity, we also need the phonon frequencies and eigenvectors at  $\mathbf{q} = \mathbf{0}$ . The point group is  $D_{2h}$ , with eight irreducible representations (irreps)<sup>21</sup>. The dynamical matrix takes a block diagonal form, with a 6×6 block corresponding to pure displacements in the  $\hat{x}$  direction ( $A$  and  $B_1$  irreps) and a 12×12 block corresponding to displacements along  $\hat{y}$  and  $\hat{z}$  ( $B_2$  and  $B_3$  irreps). The calculated frequencies of the eighteen phonons are listed in Table I with their symmetry

labels. There are five optically active phonons in Al<sub>2</sub>Ru, with symmetry labels  $B_{1u}$ ,  $B_{2u}$  and  $B_{3u}$ .

First, we calculate the real part of the optical conductivity  $\sigma_1(\omega) = \frac{\omega}{4\pi}\epsilon_2(\omega)$ , using an oscillator model<sup>22</sup>

$$\sigma_1(\omega) = \frac{e^2}{6\pi c V_0} \sum_j \frac{\gamma_j \omega^2}{(\omega_j^2 - \omega)^2 + (\gamma_j \omega)^2} S_j \quad (0.4)$$

where  $S_j$  is the oscillator strength of the  $j$ th mode

$$S_j = \sum_{\alpha=x,y,z} \left( \sum_{\beta=x,y,z} \sum_{\kappa} M_{\kappa}^{-\frac{1}{2}} Z_{\kappa,\alpha\beta}^* e_{\beta}(\kappa j) \right)^2 \quad (0.5)$$

and  $\kappa$  runs over the six atoms in the unit cell with volume  $V_0$ ,  $M_{\kappa}$  is the ion mass, and  $\omega_j$ ,  $\vec{e}(\kappa j)$ , and  $\gamma_j$  are the  $j$ th dynamical matrix eigenfrequency, eigenvector, and broadening, respectively. Since we are comparing with results from a polycrystalline sample, we sum over all modes neglecting the polarization index, and divide by 3 to average over all directions. The experimental measurement<sup>23</sup> at 300 K, shown in Fig. 3(a), includes four peaks. We associate these with the five IR-active modes expected from symmetry by assuming that the intense peak at 265 cm<sup>-1</sup> consists of two unresolved modes. The calculated frequencies thus represent underestimates of between 12% and 18% of the experimental frequencies, in parentheses: 133 cm<sup>-1</sup> (151 cm<sup>-1</sup>), 216 cm<sup>-1</sup> and 248 cm<sup>-1</sup> (265 cm<sup>-1</sup>), 279 cm<sup>-1</sup> (336 cm<sup>-1</sup>), and 353 cm<sup>-1</sup> (405 cm<sup>-1</sup>). Values of the broadening  $\gamma_1$ ,  $\gamma_2$  and  $\gamma_3$  for plotting the theoretical  $\sigma_1(\omega)$  are chosen to reproduce the intensities of the lowest two experimental peaks, with  $\gamma_4$  and  $\gamma_5$  chosen to reproduce the qualitative shape of  $\sigma_1(\omega)$  at higher frequencies (Fig. 3(b)). While the lowest calculated peak is in excellent agreement with experiment, the splitting of the second and third calculated peaks is seen to be slightly too large. In addition, their combined oscillator strength, obtained from the calculated eigenvectors, is rather too small relative to the upper two first-principles peaks. However, the calculated value for the integrated oscillator strength  $8 \int \sigma_1(\omega) d\omega$  is  $4.74 \times 10^{28} \text{s}^{-2}$ , in excellent agreement with the experimental value of  $4.94 \times 10^{28} \text{s}^{-2}$ . Since this quantity is mainly determined by  $Z_{\kappa,\alpha\beta}^*$  and is relatively insensitive to the phonon frequencies and eigenvectors, we conclude that the large first-principles values for the effective charges agree quite well with experiment.

Since the real part of the optical conductivity is independent of the dielectric tensor  $\epsilon_\infty$ , an experimental value for comparison with our calculations must be obtained from the imaginary part of the optical conductivity  $\sigma_2(\omega) = -\frac{\omega}{4\pi}\epsilon_1(\omega)$ . We fit the measured  $\sigma_2(\omega)$  below  $100 \text{ cm}^{-1}$  to  $c_1\omega + c_2\omega^2$ . Setting  $c_1 = -\frac{1}{4\pi}\bar{\epsilon}_\infty - \frac{e^2}{3V_0}\sum_j \frac{S_j}{\omega_j^2}$ , we obtain an experimental value of the polycrystalline average  $\bar{\epsilon}_\infty$  of 17, which is 18% smaller than the average of the calculated values  $\frac{1}{3}(\epsilon_{xx} + \epsilon_{yy} + \epsilon_{zz}) = 20.8$ . This overestimate is typical of the results for this quantity calculated using LDA.<sup>24</sup>

Our first-principles calculations show that large Born effective charges are an intrinsic feature of  $\text{Al}_2\text{Ru}$ , consistent with experimental observation of strong phonon absorption. However, these large charges are not the result of a static charge transfer typical of ionic compounds. Instead, given that the key role of hybridization in opening the semiconducting gap in  $\text{Al}_2\text{Ru}$  has already been established,<sup>2</sup> we propose that the hybridized nature of states near the gap is also responsible for the anomalous effective charges in  $\text{Al}_2\text{Ru}$ , in direct analogy to the perovskite oxides.<sup>6,7,8</sup> This could be more precisely formulated with a tight-binding analysis of the first-principles bandstructure<sup>25</sup>, though the necessary parametrization is complicated by the relatively low symmetry of  $\text{Al}_2\text{Ru}$ . On a more positive note, we expect that similar behavior can be observed in other semiconductors with narrow gaps opened by hybridization. Indeed, experimental indications of large phonon absorption are available for systems including  $\text{NiSnZr}$ ,<sup>26</sup>  $\text{PbTe}$ ,<sup>27</sup> and skutterudites,<sup>28</sup> and theoretical support for the non-ionic nature of the effective charges in  $\text{PbTe}$  and the other rocksalt IV-VI compounds has been obtained with the empirical pseudopotential method.<sup>29</sup> Building on first-principles investigations and tight-binding parametrizations of the bandstructures of these systems,<sup>30,31,32</sup> a general understanding of the mechanisms producing anomalous effective charges could be achieved. With a local formulation transferable to nonperiodic systems, this approach could eventually promote the interpretation of optical conductivity measurements<sup>9</sup> to elucidate the nature of vibrational modes in quasicrystals.

We thank D. N. Basov, T. Timusk, U. V. Waghmare, Ph. Ghosez, and D. Vanderbilt for useful discussions and unpublished material. We thank M. C. Payne and V. Milman for

the use of CASTEP 2.1. This work was supported by NSF Grant No. DMR-9057442. In addition, K.M.R thanks D. Vanderbilt and the Department of Physics and Astronomy of Rutgers University for their hospitality during the completion of this work, and acknowledges the support of the Clare Boothe Luce Fund and the Alfred P. Sloan Foundation.

## REFERENCES

- \* Present Address: Department of Chemical Engineering and Materials Science, University of Minnesota, 421 SE Washington Avenue, Minneapolis, MN 55455.
- <sup>1</sup> J. Evers, G. Oeklinger, and H. Mayer, *Mat. Res. Bull.* **19**, 1177 (1984).
- <sup>2</sup> D. N. Manh, G. Trambly de Laissardière, J. P. Julien, D. Mayou, and F. Cyrot-Lackmann, *Solid State Commun.* **82**, 329 (1992).
- <sup>3</sup> D. N. Basov, F. S. Pierce, P. Volkov, S. J. Poon, and T. Timusk, *Phys. Rev. Lett.* **73**, 1865 (1994).
- <sup>4</sup> G. Trambly de Laissardière, D. Nguyen Manh, L. Magaud, J. P. Julien, F. Cyrot-Lackmann, and D. Mayou, *Phys. Rev. B* **52**, 7920 (1995).
- <sup>5</sup> G. Trambly de Laissardière, Z. Dankhazi, E. Belin, A. Sadoc, D. Nguyen Manh, D. Mayou, M. A. Keegan, and D. A. Papaconstantopoulos, *Phys. Rev. B* **51**, 14035 (1995).
- <sup>6</sup> R. Resta, M. Posternak, and A. Baldereschi, *Phys. Rev. Lett.* **70**, 1010 (1993).
- <sup>7</sup> W. Zhong, R. D. King-Smith, and D. Vanderbilt, *Phys. Rev. Lett.* **72**, 3618 (1994).
- <sup>8</sup> Ph. Ghosez, X. Gonze, Ph. Lambin, and J.-P. Michenaud, *Phys. Rev. B* **51**, 6765 (1995).
- <sup>9</sup> D. N. Basov, S. J. Poon, and T. Timusk (unpublished).
- <sup>10</sup> M. C. Payne, M. P. Teter, D. C. Allan, T. A. Arias, and J. D. Joannopoulos, *Rev. Mod. Phys.* **64**, 1045 (1992).
- <sup>11</sup> D. R. Hamann, M. Schlüter, and C. Chiang, *Phys. Rev. Lett.* **43**, 1494 (1979).
- <sup>12</sup> A. M. Rappe, K. M. Rabe, E. Kaxiras, and J. D. Joannopoulos, *Phys. Rev. B* **41**, 1227 (1990).
- <sup>13</sup> L. Kleinman and D. M. Bylander, *Phys. Rev. Lett.* **48**, 1425 (1982); P. E. Blöchl, *Phys. Rev. B* **41**, 5414 (1990).

- <sup>14</sup> D. M. Ceperley and B. J. Alder, *Phys. Rev. Lett.* **45**, 566 (1980); S. H. Vosko, L. Wilk, and M. Nusair, *Can. J. Phys.* **58**, 1200 (1980).
- <sup>15</sup> S. Baroni, P. Giannozzi, and A. Testa, *Phys. Rev. Lett.* **59**, 2662 (1987).
- <sup>16</sup> X. Gonze, D. C. Allan, and M. P. Teter, *Phys. Rev. Lett.* **68**, 3603 (1992).
- <sup>17</sup> P. Villars and L. D. Calvert, *Pearson's Handbook of Crystallographic Data for Intermetallic Phases*, 2nd ed., (American Society of Metals, Metals Park, Ohio, 1991); O. Schwomma, H. Nowotny and A. Wittmann, *Monatshefte für Chemie* **94**, 924 (1963).
- <sup>18</sup> H. J. Monkhorst and J. D. Pack, *Phys. Rev. B* **13**, 5188 (1976).
- <sup>19</sup> S. E. Burkov and S. N. Rashkeev, *Solid State Commun.* **92**, 525 (1994).
- <sup>20</sup> J. N. Zemel, J. D. Jensen and A. B. Scholar, *Phys. Rev.* **140A**, 330 (1965).
- <sup>21</sup> A. P. Cracknell, *Applied Group Theory*, (Pergamon, Oxford, 1968), p. 393.
- <sup>22</sup> P. Bruesch, *Phonons: Theory and Experiments*, (Springer, New York, 1982), Vols. 1 and 2.
- <sup>23</sup> D. N. Basov and T. Timusk, private communication.
- <sup>24</sup> S. Baroni and R. Resta, *Phys. Rev. B* **33**, 7017 (1986).
- <sup>25</sup> W. A. Harrison, *Electronic Structure and the Properties of Solids*, (W. H. Freeman, San Francisco, 1980).
- <sup>26</sup> F. G. Aliev, A. I. Belogorokhov, N. B. Brandt, V. V. Kozyrkov, R. V. Skolozdra, and Yu. V. Stadnyk, *Pis'ma Zh. Eksp. Teor. Fiz.* **47**, 151 (1988) [*JETP Lett.* **47**, 184 (1988)]; Z. V. Popović, G. Kliche, R. Liu, and F. G. Aliev, *Solid State Commun.* **74**, 829 (1990).
- <sup>27</sup> E. Burstein, A. Pinczuk, and R. F. Wallis, *The physics of semimetals and narrow-gap semiconductors*, edited by D. L. Carter and R. T. Bate, (Pergamon Press, New York, 1971), p. 254.

- <sup>28</sup> G. Kliche and W. Bauhofer, *J. Phys. Chem. Solids* **49**, 267 (1988).
- <sup>29</sup> P. B. Littlewood, *J. Phys. C* **12**, 4439 (1979).
- <sup>30</sup> S. Ögüt and K. M. Rabe, *Phys. Rev. B* **51**, 10443 (1995).
- <sup>31</sup> K. M. Rabe and J. D. Joannopoulos, *Phys. Rev. B* **32**, 2302 (1985).
- <sup>32</sup> L. Nordström and D. J. Singh, *Phys. Rev. B* **53**, 1103 (1996); D. J. Singh and W. E. Pickett, *Phys. Rev. B* **50**, R11235 (1994).

## TABLES

TABLE I. The calculated phonon frequencies at  $\mathbf{q} = \mathbf{0}$ , in  $\text{cm}^{-1}$ , grouped according to the symmetry labels given in Ref. 21. The oscillator strengths  $S_j$  for the optically active modes are given in parentheses.

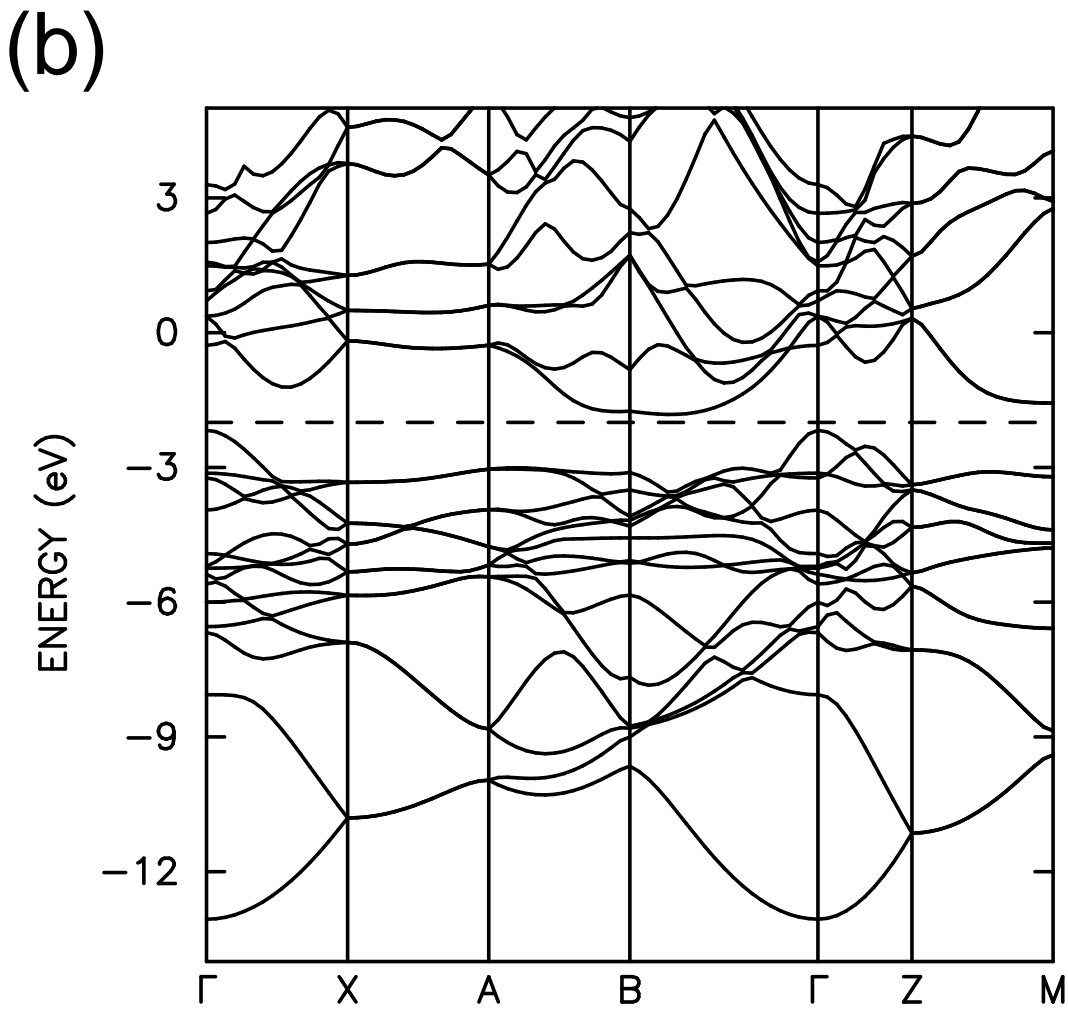
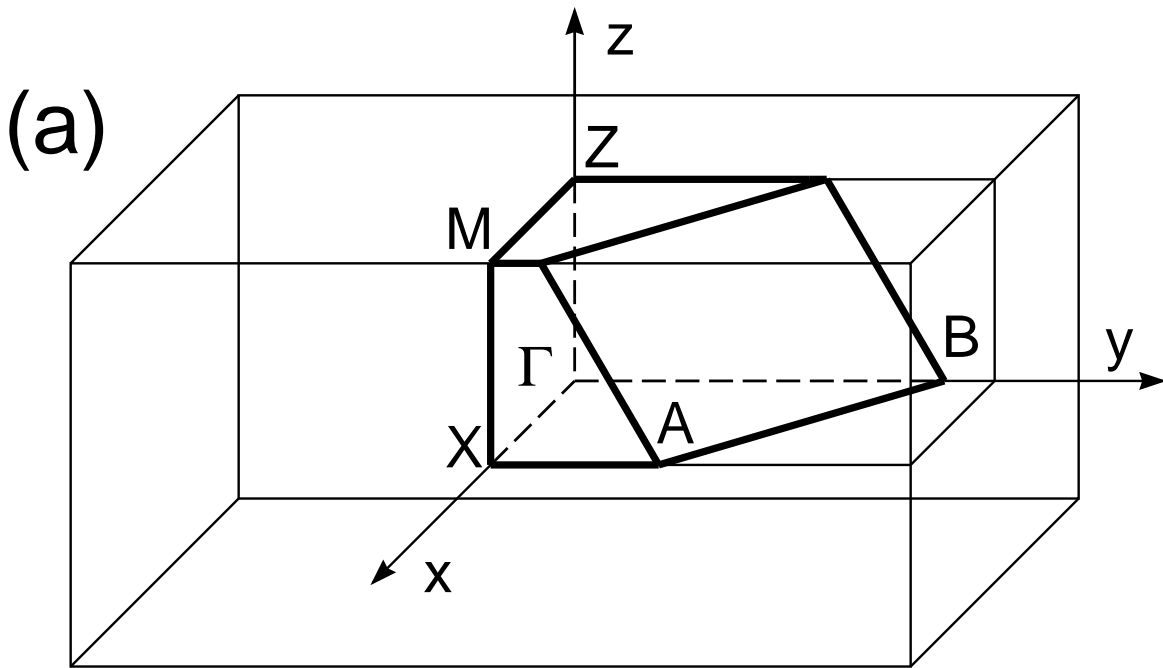
$A_g$	$B_{1g}$	$B_{2g}$	$B_{3g}$	$A_u$	$B_{1u}$	$B_{2u}$	$B_{3u}$
334	193	176	223	342	0	0	0
	225	231	344		216 (2.2)	133 (0.84)	248 (1.1)
		402	448			279 (1.9)	353 (0.67)

## FIGURES

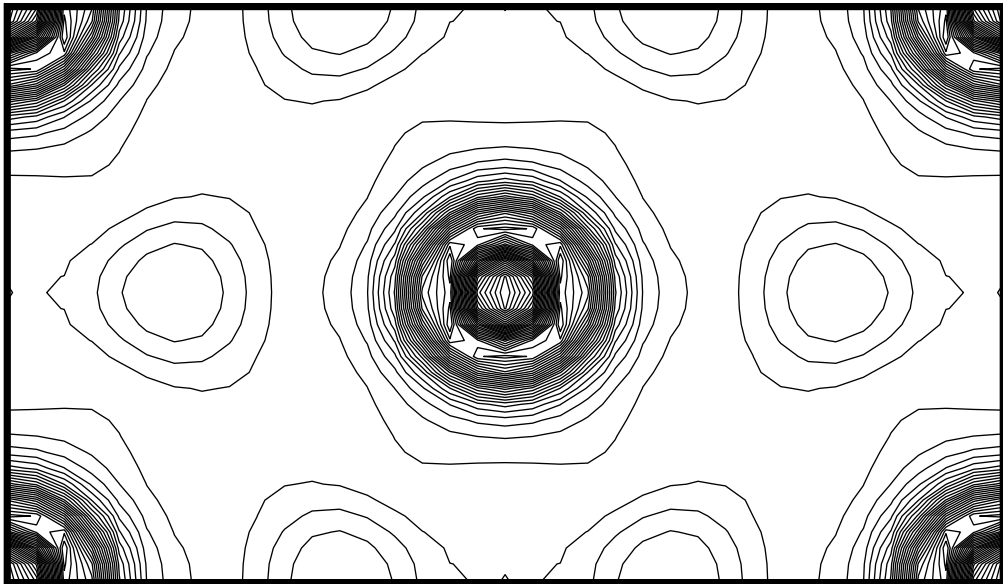
FIG. 1. (a) Irreducible wedge of the face-centered orthorhombic Brillouin zone of  $\text{Al}_2\text{Ru}$ , shown embedded in the Brillouin zone of the simple orthorhombic lattice with lattice constants  $\frac{a}{2}$ ,  $\frac{b}{2}$ ,  $\frac{c}{2}$  used in the construction of the  $\mathbf{k}$ -point sampling set. (b) Bandstructure of  $\text{Al}_2\text{Ru}$  along high-symmetry lines of the face-centered orthorhombic Brillouin zone shown in (a). The indirect gap of 0.35 eV is from the top of the valence band at  $\Gamma$  to the bottom of the conduction band along  $\Gamma - B$ .

FIG. 2. (a) Total valence charge density of  $\text{Al}_2\text{Ru}$  in the  $z = 0$  plane. The central Ru atom is surrounded by a hexagon of Al atoms. Contour intervals are  $1.3 \times 10^{-4}$  electrons per unit cell. Counting from Al towards Ru, the contour labels increase from 1 to 32, then decrease again to zero at the Ru nucleus. (b) Difference of the valence charge density (a) from that of superimposed free neutral atoms (Al  $s^2p$  and Ru  $d^7s^1$ ). Contour intervals are 1/3 of those in (a), with dashed lines indicating negative contour values. Counting outward from Al, the first few contour labels are -2, -2, -1, 0, 1 and 2.

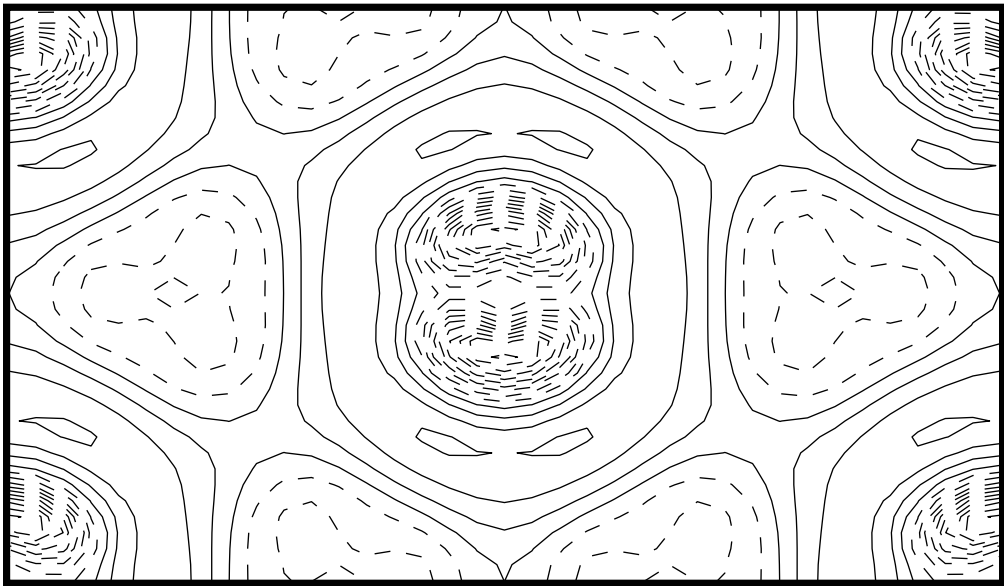
FIG. 3. The real part of the optical conductivity of  $\text{Al}_2\text{Ru}$ , in  $(\Omega \text{ cm})^{-1}$ : (a) experimental measurement at 300 K (Ref. 9); (b) theoretical prediction. In (b), a background of  $50 (\Omega \text{ cm})^{-1}$  has been added and values of  $\gamma_j = 25, 9.0, 4.5, 65$  and  $50 \text{ cm}^{-1}$  ( $j = 1, \dots, 5$ ) chosen as described in the text.



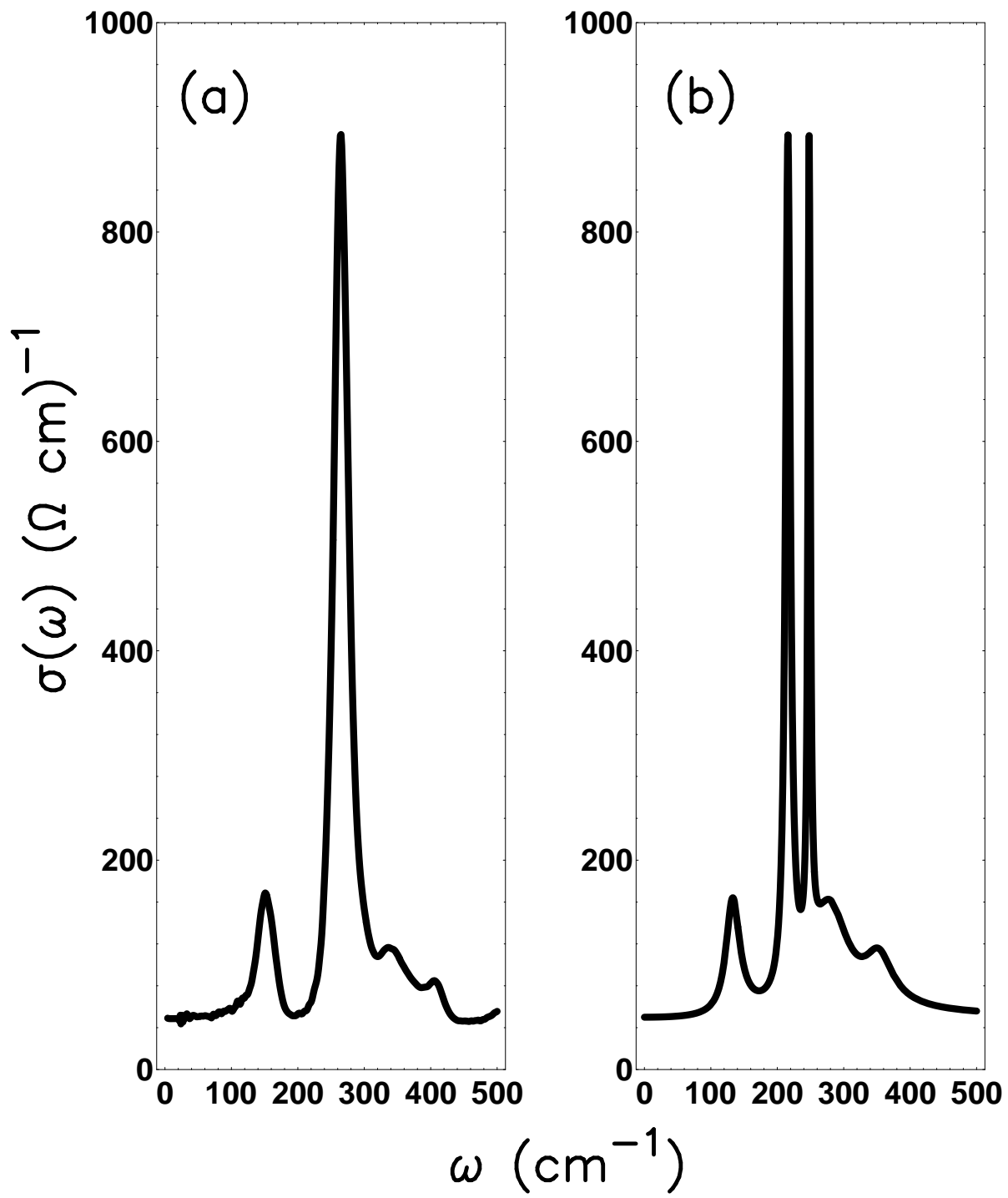
*Ogut and Rabe, Figure 1*



*Ogut and Rabe, Figure 2(a)*



*Ogut and Rabe, Figure 2(b)*



*Ogut and Rabe, Figure 3*